

1

2 **Supplementary Information for**

3 **The Ferroelectric Photo-Groundstate of SrTiO₃ : Cavity Materials Engineering**

4 **Simone Latini, Dongbin Shin, Shunsuke A. Sato, Christian Schäfer, Umberto De Giovannini, Hannes Hübener and**
5 **Angel Rubio**

6 **E-mail: simone.latini@mpsd.mpg.de, angel.rubio@mpsd.mpg.de**

7 **This PDF file includes:**

- 8 Supplementary text
- 9 Figs. S1 to S2
- 10 SI References

11 Supporting Information Text

12 1. QED Hamiltonian

13 In order to predict the properties of SrTiO₃ embedded in an optical cavity we introduce the following atomistic quantum
14 electrodynamical (QED) Hamiltonian (1):

$$15 \quad \hat{H} = \omega_c \hat{a}^\dagger \hat{a} + \frac{\hat{p}_c^2}{2M_c} + \frac{1}{2M_f} [\hat{p}_f - A_0 Z_f (\hat{a}^\dagger + \hat{a})]^2 + V_{\text{DFT}}(\hat{Q}_c, \hat{Q}_f), \quad [1]$$

16 where ω_c is the frequency of the photons in the cavity which is set by the cavity length L_\perp , a^\dagger and a are the corresponding creation
17 and annihilation operators, $A = A_0(a^\dagger + a)$ is the cavity vector potential, $M_c = 111492$ a.u. and $M_f = 194059$ a.u. the effective
18 masses of the lattice vibration (sum of the masses of the atoms in the unit cell) and the ferroelectric soft (FES) mode respectively,
19 Z_f the Born effective charge of the FES mode and $V_{\text{DFT}}(Q_c, Q_f) = \sum_{i=1}^6 k_{f,i} \hat{Q}_f^{2i} + \sum_{j=2}^5 k_{c,j} \hat{Q}_c^j + \sum_{i=1}^6 \sum_{j=1}^5 k_{fc,i,j} \hat{Q}_f^{2i} \hat{Q}_c^j$
20 the potential energy surface shown in Fig. 1(c) of the main text, which includes the intrinsic phonon non-linearities of SrTiO₃.
21 The FES and lattice modes are parameterized in terms Q_f and Q_c respectively (see next section for more details on Q_f . The
22 Born effective charges and the 2D potential energy surface expansion coefficients k are determined within DFT (density
23 functional theory) using the Perdew-Burke-Ernzerhof (PBE) functional (2) as described in Ref. (3). Furthermore, we assume
24 the Born-effective charge Z_f to be not affected by the light-matter coupling. We stress that in the Hamiltonian it is essential to
25 take into account the diamagnetic as it guarantees the existence of a groundstate bound from below (4). It is important to note
26 that in the Hamiltonian above we reduced the phononic degrees of freedom of SrTiO₃ to the FES mode and lattice vibration
27 only and it is effectively describing a single unit cell. The unit cell Hamiltonian is effectively describing the collective Γ -phonon
28 modes coupled with the dipole component of the electromagnetic fields. As shown in Ref. (3), this two modes are sufficient to
29 correctly describes the physics of SrTiO₃ by demonstrating quantum paraelectricity and proving the correct behaviour of FES
30 mode for an extended range of temperatures.

31 The strength of the cavity light-phonon coupling is determined by the Born effective charge and the photon mode amplitude
32 A_0 . For the Γ -phonon mode coupled to the dipole component of the electromagnetic field the mode amplitude is given by (5, 6):

$$33 \quad A_0 = \sqrt{\frac{d_\perp}{2\pi c v}} \quad [2]$$

34 with d_\perp and v the thickness of the SrTiO₃ slab and the volume of the unit cell respectively, c the speed of light and we used
35 the relation $L_\perp = \pi c / \omega_c$ where L_\perp is the vertical dimension of the cavity. In order to obtain the expression above we took into
36 account the difference in the thickness of the cavity and the material, i.e. $V_c = V_{\text{SrTiO}_3} * L_\perp / d_\perp$. The scaling of the mode
37 volume above with the thickness of the SrTiO₃ crystal provides a direct way to increase the coupling of the cavity increasing
38 the amount of material.

39 2. Parameterization of Lattice Mode

40 In the atomistic Hamiltonian shown in the previous section we have conveniently decided to parameterize the FES mode with
41 the distance between the Ti and O atoms along the c-axis, as this distance is ultimately involved in the definition of the unit
42 cell dipole: $|\vec{D}| \equiv Z_f d_{\text{Ti-O}}$. The particular choice however implies that the effective mass M_f and Born effective charge Z_f have
43 to be rescaled accordingly as compared to the corresponding quantities for the FES phonon mode. This is because, even if of
44 minor importance, the FES phonon mode involves the motion of all the other atoms in the unit cell. Since within density
45 functional perturbation theory with the PBE functional (DFPT@PBE) (7) the FES mode has an imaginary frequency, the
46 phonon mode is ill defined and therefore we evaluated such mode directly from the difference of the atomic position in the
47 optimized paraelectric and ferroelectric geometry. Specifically, we defined the FES eigenvector as:

$$48 \quad \vec{U}_I^f = \frac{\vec{s}_I^{\text{ferro}} - \vec{s}_I^{\text{para}}}{\sum_J |\vec{s}_J^{\text{ferro}} - \vec{s}_J^{\text{para}}|}, \quad [3]$$

49 where I is the index running over the atoms of the unit cell and \vec{s} are the atomic basis vectors of the two different geometries.
50 The eigenvector above and Q_f are then related by:

$$51 \quad Q_f = x_f (U_{\text{Ti},z}^f - U_{\text{O},z}^f) \quad [4]$$

52 with x_f the actual FES mode parameter, i.e. the one that is independent of the specific atoms and to which the phonon
53 effective masses and Born effective charges are standardly referred to. To calculate the effective mass and charge for the Q_f
54 parameter, the following formula can be applied:

$$55 \quad M_f = \sum_I M_I \left(\frac{U_{I,z}^f}{U_{\text{Ti},z}^f - U_{\text{O},z}^f} \right)^2$$

$$Z_f = \sum_a Z_I \left(\frac{U_{I,z}^f}{U_{\text{Ti},z}^f - U_{\text{O},z}^f} \right), \quad [5]$$

56 where M_I and Z_I are the atomic mass and the Born effective charge for the atom I .

57 We set up our atomistic Hamiltonian for the SrTiO₃, outside the cavity, with the quantities defined above calculated using
58 the PBE functional. The full diagonalization of the Hamiltonian is performed on a simple product basis set $|Q_f\rangle \otimes |Q_c\rangle \otimes |n\rangle$
59 which consists of a 50×25 real space grid for the phononic coordinates Q_f and Q_c and up to $n = 9$ Fock number states as a
60 basis for the photons. We obtain a FES mode frequency of 0.44 THz, which reproduces well the experimental results (8–10).

61 3. Characterization of the Ferroelectric Photo-Groundstate

62 In the main text we characterized the photo-groundstate of SrTiO₃ in terms of the generalized FES mode frequency, mean
63 displacement of the lattice vibration and Von Neumann entropy of the photonic sub-system. The latter quantity is commonly
64 used to describe the amount of correlation between a given sub-system and all the others, which in our case is just the phononic
65 system. The Von Neumann entropy is defined as:

$$66 \quad \mathcal{S} = -\eta_i \sum_i \eta_i \log(\eta_i), \quad [6]$$

67 where η_i are the eigenvalues of the density matrix of the chosen subsystem, which for the photons is defined as:

$$68 \quad \hat{\rho}_{\text{ph}} = \text{Tr}_{\text{pn}} [\hat{\rho}_{\text{full}}], \quad [7]$$

69 with Tr_{pn} meant as the trace over the phononic states. The resulting photonic entropy is the one shown in Fig. 2(c) of the
70 main text.

71 To further characterize the photo-groundstate of SrTiO₃, we report the expectation value of the squared FES mode
72 displacement, the purity and the expectation value of the photon number. These quantities are shown in Fig. S1 as a function
73 of the coupling strength. We point out that the maximum of the mean squared displacement $\langle \hat{Q}_f^2 \rangle$ is at $\omega_c = 3$ THz, which is
74 off-resonant with the FES mode frequency.

75 The existence of an optimal for $\langle \hat{Q}_f^2 \rangle$ is a consequence of the trade-off between the delocalization and the dipole matrix elements
76 between the phononic states coupled by the cavity photons. Indeed the higher ω_c , the higher the phononic excited states
77 that are coupled to the groundstate. In turns, this means that resulting delocalization gets larger but at the same time the
78 dipole-matrix element becomes smaller.

79 Beside the Von Neumann entropy another way to characterize the correlation between light and matter is to evaluate the
80 so-called purity (11). This is defined as follows:

$$81 \quad \gamma = \text{Tr} [\hat{\rho}_{\text{ph}}^2]. \quad [8]$$

82 A purity value that deviates from 1 means that the groundstate cannot be factorized in a simple tensor product of a phononic
83 and photonic wavefunction, hence light and matter are correlated. In the context of correlated systems, another informative
84 quantity is the so called inverse participation ratio (IPR). The IPR gives a measure of localization and it is defined as
85 $\sigma = \sum_x \rho(x)^2$ with $\rho(x)$ the density of the system on a given space x . We calculated the IPR for the ferroelectric mode (we
86 integrated out the Q_c dimension) with and without light-matter coupling for a cavity frequency of 3 THz: we found that the
87 ferroelectric mode is more localized and the IPR ratio is $\sigma_{A_0=0.3}/\sigma_{A_0=0} = 0.017$.

88 Finally, the finite expectation value of the photon number operator $N_{\text{ph}} = \langle \hat{a}^\dagger \hat{a} \rangle$ on the groundstate justifies the use of the term
89 photo-groundstate. Indeed, even if the cavity is dark, there is a finite number of photons generated by the presence of SrTiO₃.

90 4. Dynamical Localization induced by Vacuum Fluctuations

91 In this section, we describe an alternative analytic simple approach to extend the theory of dynamical localization to the case
92 of the quantized light field in a cavity (12, 13).

93 **A. Effective Hamiltonian.** The eigenvalue problem associated with the QED Hamiltonian in the first section can be rewritten in
94 the following matrix form:

$$95 \quad \begin{pmatrix} H_0 & H_1 & 0 & 0 & 0 & \dots \\ H_1^\dagger & H_0 + \omega & \sqrt{2}H_1 & 0 & 0 & \dots \\ 0 & \sqrt{2}H_1^\dagger & H_0 + 2\omega & \sqrt{3}H_1 & 0 & \dots \\ \vdots & \ddots & \ddots & \ddots & \vdots & \ddots \end{pmatrix} \begin{pmatrix} u_0 \\ u_1 \\ u_2 \\ \vdots \end{pmatrix} = E \begin{pmatrix} u_0 \\ u_1 \\ u_2 \\ \vdots \end{pmatrix} \quad [9]$$

96 where H_0 and H_1 are matrices in the matter basis (see below) and u_i are photon components of the eigenstate. The action on
97 the n -th photon-sector can be written as

$$98 \quad \sqrt{n}H_1^\dagger u_{n-1} + (H_0 + n\omega)u_n + \sqrt{n+1}H_1 u_{n+1} = E u_n, \quad [10]$$

99 which can be proven by inspection. From this, one can recursively write the action of the full Hamiltonian matrix into a single
100 photon sector in the form $H_{\text{eff}}|u_0\rangle = E|u_0\rangle$ and thus get an approximation for the groundstate (or low lying eigenvalues). The
101 effective Hamiltonian can be easily shown to be:

$$102 \quad H_{\text{eff}} = H_0 - H_1 \frac{1}{H_0 + \omega - E - 2H_1 \frac{1}{H_0 + 2\omega - E + \dots} H_1^\dagger} H_1^\dagger. \quad [11]$$

103 **B. High frequency Approximation.** How many photon sectors need to be included depends on the ratio between light-matter
104 coupling and frequency. To make this clear we write $H_1 = A_0 P \tilde{H}_1$ and factorize:

$$105 \quad H_{\text{eff}} = H_0 - \frac{(A_0 P)^2}{\omega} \tilde{H}_1 \frac{1}{1 + \frac{H_0 - E}{\omega} - 2 \frac{(A_0 P)^2}{\omega} \tilde{H}_1 \frac{1}{H_0 + 2\omega - E} \tilde{H}_1^\dagger} \tilde{H}_1^\dagger \quad [12]$$

106 Only if $\omega \gg A_0 P$ the continued fractions can be neglected and the leading term reads

$$107 \quad H_{\text{eff}} = H_0 - \frac{A_0^2 P^2}{\omega} \tilde{H}_1 \frac{1}{1 + \frac{H_0 - E}{\omega}} \tilde{H}_1^\dagger = H_0 - H_1 [H_0 + \omega - E]^{-1} H_1^\dagger, \quad [13]$$

108 as in the main text A_0 defines the photon mode volume and P is a c-number that sets the scale of the photon-phonon momentum
109 matrix. Under this condition we can use the resolvent as a Neumann series and write

$$110 \quad H_{\text{eff}} = H_0 - H_1 \sum_{n=0}^{\infty} \frac{(H_0 - E)^n}{\omega^{n+1}} H_1^\dagger. \quad [14]$$

111 The Neumann series converges for $\omega > \max(\{E_{0\lambda}\}) - E$, where $H_0 \psi_\lambda = E_{0\lambda} \psi_\lambda$, but Eq. (14) is only a valid approximation for
112 the full Hamiltonian as long as the truncation at $n = 1$ is possible.

113 The series formulation of the effective Hamiltonian is useful because it yields to leading order in $1/\omega$:

$$114 \quad H_{\text{eff}}^{(1)} \approx H_0 - \frac{H_1 H_1^\dagger}{\omega} \quad [15]$$

115 which can be readily solved. For all higher orders the effective Hamiltonian gives self-consistent eigenvalue equation that can
116 only be solved iteratively. However, one can approximate this self-consistency by considering the linearization $E \rightarrow E_0$. To
117 second order in $1/\omega$ the effective Hamiltonian for the i th eigenstate then reads

$$118 \quad H_{\text{eff},i}^{(2)} \approx H_0 - \frac{H_1 H_1^\dagger}{\omega} + \frac{H_1 H_0 H_1^\dagger}{\omega^2} - \frac{H_1 E_{0i} H_1^\dagger}{\omega^2} \quad [16]$$

119 which has to be solved separately for each eigenstate.

120 **C. Localisation in SrTiO₃.** To describe the photon induced localization we consider the system within a two-level approximation.
121 We choose as the two levels, two Gaussians which are localized in the left and right well of the 1D FES mode energy potential
122 respectively. In matrix form this translates to:

$$123 \quad H = \begin{pmatrix} 0 & t \\ t & 0 \end{pmatrix} + A_0 P \begin{pmatrix} 0 & -i \\ i & 0 \end{pmatrix} (a + a^\dagger) + \omega a^\dagger a \quad [17]$$

124 so that $H_0 = t\sigma_x$ and $H_1 = A_0 P\sigma_y$. Here P is directly the L-R momentum matrix element. The high frequency approximation
125 from the previous subsection then reads:

$$126 \quad H_{\text{eff}} = \left(t - \frac{A_0^2 P^2 t}{\omega^2} \right) \sigma_x - \left(\frac{A_0^2 P^2}{\omega} + \frac{A_0^2 P^2 E_0}{\omega^2} \right) \mathbf{1}. \quad [18]$$

127 The second term is only shifting the eigenvalues, while the first one gives full localisation if $\frac{A_0^2 P^2}{\omega^2} = 1$. In that case the
128 effective Hamiltonian has degenerate eigenvalues and similar to the full phonon-QED case one can make linear combinations of
129 eigenvectors that give (1, 0) and (0, 1).

130 5. Temperature Dependent Response Function

131 In order to calculate the phase diagram that we presented in the main text, we need to include the effect of temperature in our
132 theory. To do so we apply Kubo's formula for the linear response of a thermal state to a perturbation described by:

$$133 \quad \hat{H}'(t) = -Z_f \hat{Q}_f E(t) \quad [19]$$

134 where Z_f , the FES mode effective charge, is assumed to be temperature independent. Applying Kubo's formula, the resulting
135 polarizability takes the form:

$$136 \quad \chi(\omega, T, A_0) = - \sum_{i,j} \rho_i(T, A_0) Z_f^* |D_{ij}(A_0)|^2 \times \left\{ \frac{1}{[\epsilon_j(A_0) - \epsilon_i(A_0)] - \omega - i\delta} + \frac{1}{[\epsilon_j(A_0) - \epsilon_i(A_0)] + \omega + i\delta} \right\}, \quad [20]$$

137 where the dipole matrix and the thermal density matrix are defined as $D_{ij}(A_0) = \langle \psi_i(A_0) | \hat{Q}_f | \psi_j(A_0) \rangle$ and $\rho_i(T, A_0) =$
138 $e^{-[\epsilon_i(A_0) - \epsilon_0(A_0)]/k_B T} / \sum_j e^{-[\epsilon_j(A_0) - \epsilon_0(A_0)]/k_B T}$, respectively and $|\psi_i(A_0)\rangle$ are the eigenstates of the QED Hamiltonian for

139 different values of the cavity coupling. Such a response function for SrTiO₃ is shown in Fig. S2 for different temperatures and
140 cavity coupling strengths. Note that the artificial broadening δ is kept constant with temperature however the increase in
141 temperature introduces a finite population in the excited states which explains the appearance of further peaks.

142 We then define a characteristic temperature dependent FES mode frequency from such a response function as:

$$143 \quad \omega(T, A_0) = \frac{\int d\omega \omega \operatorname{Im}[\chi(\omega, TA_0)]}{\int d\omega \operatorname{Im}[\chi(\omega, T, A_0)]}. \quad [21]$$

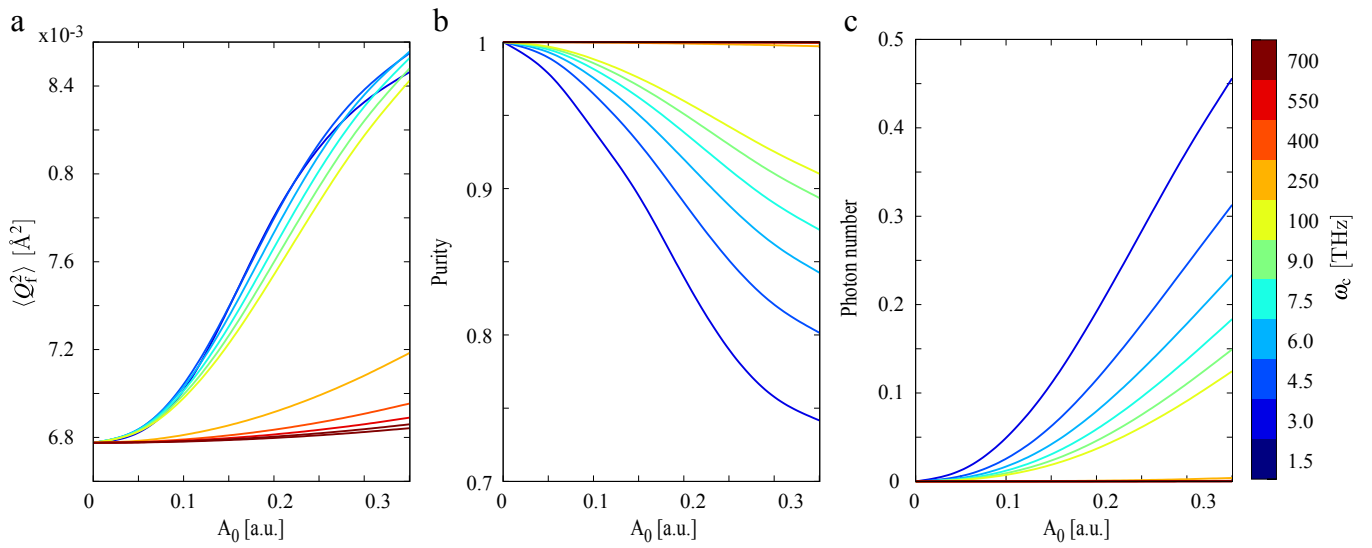


Fig. S1. Dependence of the microscopic properties of SrTiO₃ on the cavity parameters. (a) mean squared displacement of the generalized ferroelectric soft mode as a function of the cavity coupling and photon energy. Note that by the symmetry of the 2D potential energy surface the expectation value of the ferroelectric soft mode displacement has to be zero. (b) Purity of the photo-groundstate as a measure of light-matter correlation. (c) Expectation value of the number of photons.

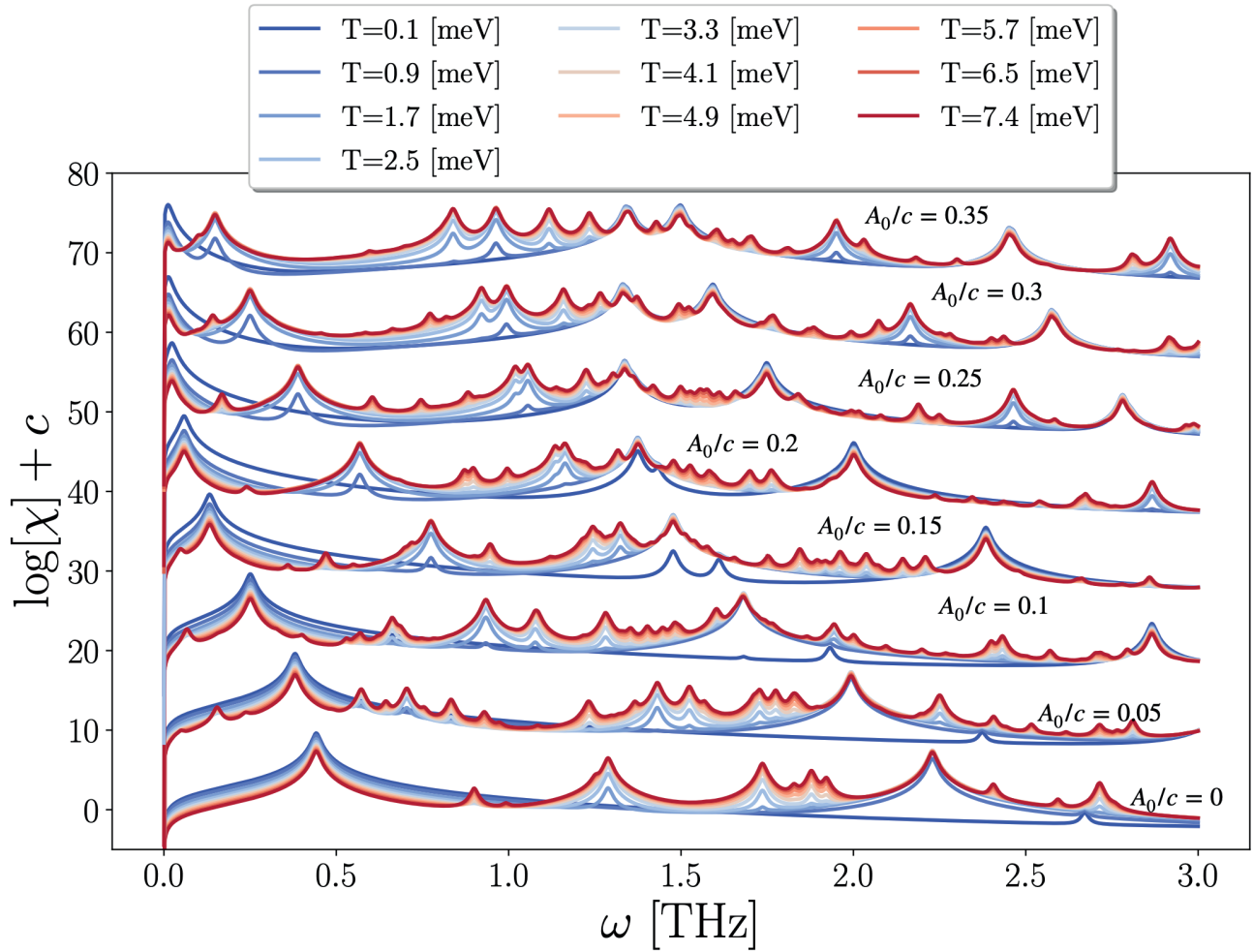


Fig. S2. Dependence of the imaginary part of the response function on temperature and cavity coupling strength. The response to a probing electric field is calculated within Kubo's linear response theory. The values are shown in logarithmic scale and they are shifted by a constant for clarity.

144 **References**

- 145 1. M Ruggenthaler, N Tancogne-Dejean, J Flick, H Appel, A Rubio, From a quantum-electrodynamical light–matter
146 description to novel spectroscopies. *Nat. Rev. Chem.* **2**, 1–16 (2018).
- 147 2. JP Perdew, K Burke, M Ernzerhof, Generalized gradient approximation made simple. *Phys. Rev. Lett.* **77**, 3865–3868
148 (1996).
- 149 3. D Shin, et al., The quantum paraelectric phase of SrTiO₃ from first principles. *arXiv preprint arXiv:2101.02291* (2021).
- 150 4. V Rokaj, DM Welakuh, M Ruggenthaler, A Rubio, Light–matter interaction in the long-wavelength limit: no ground-state
151 without dipole self-energy. *J. Phys. B: At. Mol. Opt. Phys.* **51**, 034005 (2018).
- 152 5. Y Ashida, et al., Quantum electrodynamic control of matter: Cavity-enhanced ferroelectric phase transition. *Phys. Rev. X*
153 **10**, 041027 (2020).
- 154 6. MA Sentef, M Ruggenthaler, A Rubio, Cavity quantum-electrodynamical polaritonically enhanced electron-phonon
155 coupling and its influence on superconductivity. *Sci. Adv.* **4**, eaau6969 (2018).
- 156 7. X Gonze, C Lee, Dynamical matrices, Born effective charges, dielectric permittivity tensors, and interatomic force constants
157 from density-functional perturbation theory. *Phys. Rev. B* **55**, 10355–10368 (1997).
- 158 8. G Shirane, Y Yamada, Lattice-dynamical study of the 110 K phase transition in SrTiO₃. *Phys. Rev.* **177**, 858 (1969).
- 159 9. A Yamanaka, et al., Evidence for competing orderings in strontium titanate from hyper-Raman scattering spectroscopy.
160 *Eur. Lett.* **50**, 688–694 (2000).
- 161 10. H Vogt, Refined treatment of the model of linearly coupled anharmonic oscillators and its application to the temperature
162 dependence of the zone-center soft-mode frequencies of KTaO₃ and SrTiO₃. *Phys. Rev. B* **51**, 8046–8059 (1995).
- 163 11. J Flick, M Ruggenthaler, H Appel, A Rubio, Kohn-Sham approach to quantum electrodynamic density-functional theory:
164 Exact time-dependent effective potentials in real space. *Proc. Natl. Acad. Sci.* **112**, 15285–15290 (2015).
- 165 12. DH Dunlap, VM Kenkre, Dynamic localization of a charged particle moving under the influence of an electric field. *Phys.*
166 *Rev. B* **34**, 3625–3633 (1986).
- 167 13. MA Sentef, J Li, F Künzel, M Eckstein, Quantum to classical crossover of Floquet engineering in correlated quantum
168 systems. *Phys. Rev. Res.* **2**, 033033 (2020).